LETTER https://www.nature.com/articles/nature13700

doi:10.1038/nature13700

# Lithium–antimony–lead liquid metal battery for grid-level energy storage

Kangli Wang[1], Kai Jiang[1], Brice Chung[1], Takanari Ouchi[1], Paul J. Burke[1], Dane A. Boysen[1], David J. Bradwell[1], Hojong Kim[1], Ulrich Muecke[1] & Donald R. Sadoway[1]

**The ability to store energy on the electric grid would greatly improve its efficiency and reliability while enabling the integration of intermittent renewable energy technologies (such as wind and solar) into baseload supply[1–4]. Batteries have long been considered strong candidate solutions owing to their small spatial footprint, mechanical simplicity and flexibility in siting. However, the barrier to widespread adoption of batteries is their high cost. Here we describe a lithium–antimony–lead liquid metal battery that potentially meets the performance specifications for stationary energy storage applications. This Li||Sb–Pb battery comprises a liquid lithium negative electrode, a molten salt electrolyte, and a liquid antimony–lead alloy positive electrode, which self-segregate by density into three distinct layers owing to the immiscibility of the contiguous salt and metal phases. The all-liquid construction confers the advantages of higher current density, longer cycle life and simpler manufacturing of large-scale storage systems (because no membranes or separators are involved) relative to those of conventional batteries[5,6]. At charge–discharge current densities of 275 milliamperes per square centimetre, the cells cycled at 450 degrees Celsius with 98 per cent Coulombic efficiency and 73 per cent round-trip energy efficiency. To provide evidence of their high power capability, the cells were discharged and charged at current densities as high as 1,000 milliamperes per square centimetre. Measured capacity loss after operation for 1,800 hours (more than 450 charge–discharge cycles at 100 per cent depth of discharge) projects retention of over 85 per cent of initial capacity after ten years of daily cycling. Our results demonstrate that alloying a high-melting-point, high-voltage metal (antimony) with a low-melting-point, low-cost metal (lead) advantageously decreases the operating temperature while maintaining a high cell voltage. Apart from the fact that this finding puts us on a desirable cost trajectory, this approach may well be more broadly applicable to other battery chemistries.**

Among metalloids and semi-metals, Sb stands as a promising positive-electrode candidate for its low cost (US$1.23 mol$^{-1}$) and relatively high cell voltage when coupled with an alkali or alkaline-earth negative electrode[5]. In previous work[6], we demonstrated the performance of a Mg||Sb liquid metal battery at current densities ranging from 50 to 200 mA cm$^{-2}$, achieving a round-trip energy efficiency of up to 69%. However, the high melting points of Mg ($T_m$ = 650 °C) and Sb ($T_m$ = 631 °C) require the cell to operate near 700 °C. A high operating temperature is undesirable because it results in higher rates of corrosion and detracts from overall storage efficiency, which ultimately increases cost of ownership. These potential limitations, in conjunction with an estimated electrode materials cost of US$375 kWh$^{-1}$ and an average cell voltage of 0.21 V (measured under galvanostatic discharge at 200 mA cm$^{-2}$), render Mg||Sb cells impractical for commercial applications[5].

With an average cell voltage of 0.92 V, the Li||Sb combination is an appealing alternative[7]. Moreover, Li melts at 180 °C and exhibits low solubility in lithium halide melts, which results in lower self-discharge current and, hence, higher energy efficiency especially when compared with sodium alternatives[8]. Despite these attractive properties, the high melting point of Sb sets the operating temperature of the Li||Sb cell at almost 500 °C above the melting point of Li. Although alloying Sb with another metal can be an effective strategy to lower the melting point of the positive electrode, this is generally accompanied by an undesirable decrease in cell voltage, as observed in the Mg||Sn–Sb (ref. 9) and Na||Bi–Sb systems (ref. 10).

Here we report that, with the use of a Li negative electrode, the addition of Pb to Sb maintains a cell voltage almost as great as that for pure Sb while substantially reducing the melting temperature (eutectic composition, Sb–Pb 18:82 mol%; melting temperature, $T_m$ = 253 °C; ref. 11). Figure 1 shows the equilibrium voltage of the Li||Sb–Pb cell as a function of Li concentration in various Sb–Pb alloys. Measurements were made by coulometric titration in a LiF–LiCl–LiI molten salt electrolyte

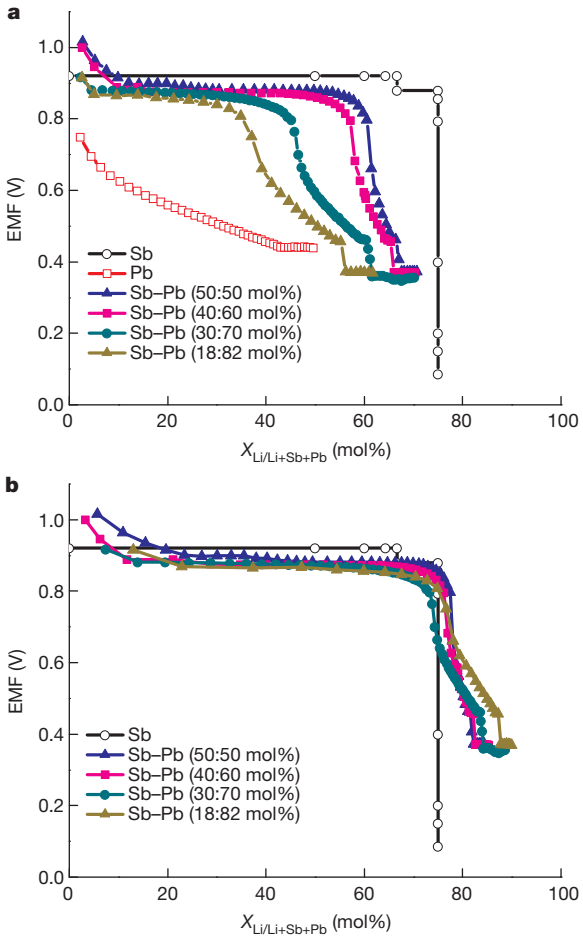


**Figure 1 | Electromotive force of Li–Sb–Pb electrodes measured by coulometric titration at 450 °C.** Electromotive force (EMF) as a function of Li concentration in Sb–Pb alloys (**a**), and as a function of Li concentration normalized with respect to Sb (**b**). Pure Sb data are from ref. 7.

[1]Department of Materials Science and Engineering, Massachusetts Institute of Technology, 77 Massachusetts Avenue, Cambridge, Massachusetts 02139-4307, USA.

(20:50:30 mol%, $T_m = 430\ ^\circ C$). Four compositions of Sb–Pb alloys are shown here: 50:50, 40:60, 30:70 and 18:82 mol% (eutectic composition). The corresponding equilibrium voltages of the binary Li||Sb cell[12] and the binary Li||Pb cell[13] are also shown for comparison. At the chosen experimental temperature (450 °C), Sb–Pb alloys and pure Pb are liquid, whereas Sb is solid. As shown in Fig. 1, the Li||Sb (solid) chemistry has the highest cell voltage, at 0.92 V, and the Li||Pb chemistry exhibits the lowest cell voltage, just under 0.6 V. We note that even at high dilution (up to 82 mol% Pb in Sb), the Li||Sb–Pb systems operate at cell voltages very near Li||Sb levels (only about 0.05 V lower), indicating that the Li||Sb–Pb electrode potential is determined primarily by the Li–Sb interaction. To reveal the predominant role of Sb in setting the potential, Fig. 1b was normalized to the concentration of Li relative to Sb. Figure 1b shows that all Li–Sb–Pb electrodes share a behaviour similar to that of the Li–Sb electrode: in each case, a region of near-constant, high potential is followed by a drop in potential at 75 mol% Li relative to Sb. This behaviour is suggestive of the Li||Sb system in which $Li_xSb$ ($x < 3$) compounds are formed and thereby generate a high electrode potential relative to pure Li. When the concentration of the alloy reaches 75 mol% Li in Sb, a low-potential $Li_3Sb$ phase is formed, and the cell voltage drops precipitously[7].

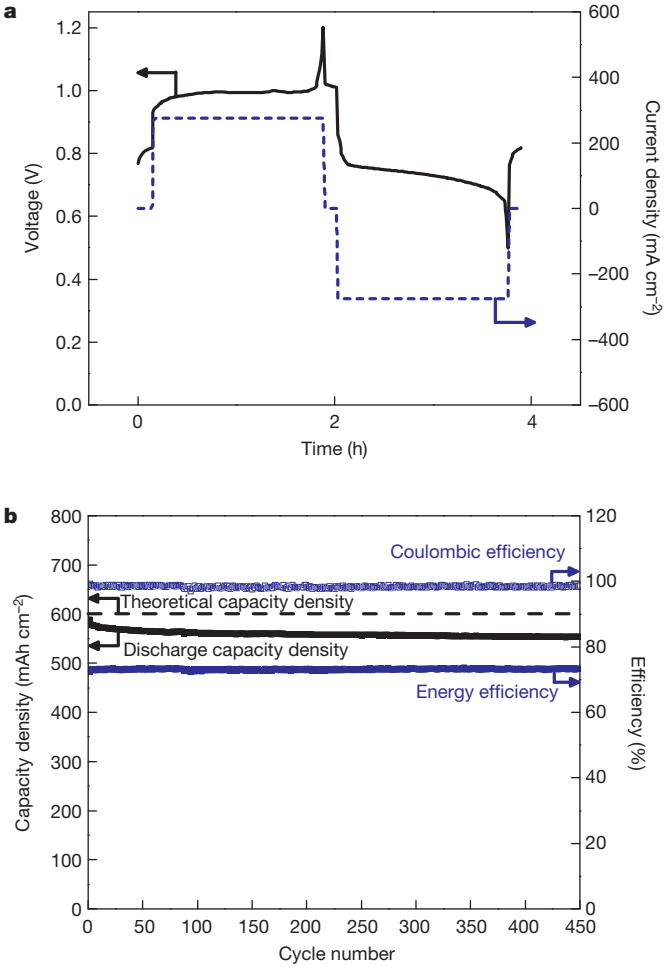


**Figure 2 | Performance of a Li||Sb–Pb cell cycled at 275 mA cm$^{-2}$.** **a**, Profiles of voltage and current density during charge–discharge (15th cycle). The results derive from measurements on more than 10 cells. **b**, Coulombic efficiency, energy efficiency and discharge capacity density as functions of cycle number. The theoretical cell capacity was 1.9 Ah with a fully discharged target composition of 45% Li in an Sb–Pb 30:70 mol% alloy (3.16 cm$^2$ of active surface area). The operating temperature was 450 °C. The results derive from measurements on more than two cells.

Cell performance was demonstrated in 1.9 Ah theoretical capacity cells (3.16 cm$^2$ positive-electrode/electrolyte interfacial area) fitted with a Li negative electrode, an Sb–Pb positive electrode (30–70 mol%) and a LiF–LiCl–LiI molten salt electrolyte (20:50:30 mol%, $T_m = 430\ ^\circ C$). Cells were assembled in the fully charged state in an Ar-filled glove box, placed inside a sealed test vessel and operated in a vertical tube furnace at 450 °C. When the temperature exceeded the melting point of the salt, the equilibrium cell voltage stabilized at ~1.0 V, consistent with titration results. At a stepped-potential of 1.2 V, the self-discharge current was measured to be 0.6 mA cm$^{-2}$, which is significantly lower than the value observed in Na systems[8] (20 mA cm$^{-2}$). This is attributable to the lower solubility of Li in its molten halides[14]. A typical charge–discharge voltage profile and the usual performance metrics as functions of cycle index are shown in Fig. 2. At a high current density of 275 mA cm$^{-2}$, cells consistently achieved 93% of their theoretical capacity. The nominal discharge voltage was 0.73 V, which is more than three times higher than that of Mg||Sb. On the basis of measured cell performance, the electrode materials costs are estimated to be US$68 kWh$^{-1}$, which is about one-fifth of the value for Mg||Sb cells.

For stationary applications, long service lifetime is a critical factor. Liquid metal batteries are advantageous owing to the liquid electrodes and molten salt electrolyte, which avoid many of the common failure mechanisms associated with batteries fitted with solid-state electrodes, for example undesirable film formation at the electrode–electrolyte interface, or phase transformations that mechanically damage cell components[15]. Here we show the results of charge–discharge cycle testing of the Li||Sb–Pb system (Fig. 2b). Over the duration of the test, the cells exhibited a Coulombic efficiency of 98% and a round-trip energy efficiency of 73%, maintaining 94% of the initial capacity after 450 cycles at full depth of discharge. The capacity fade rate decreased after the 100th cycle, whereupon the fade rate between the 100th and 450th cycles was 0.004% per cycle. This is equivalent to retention of over 85% of the initial capacity after ten years of daily cycling. Cross-sections of cells after 1,800 hours of operation did not exhibit any obvious corrosion of cell components (current collectors and walls).

The ability to operate at high current densities with minimal impact on cycle life is an asset for certain grid applications such as ancillary services. Here we show the capability of Li||Sb–Pb cells with a LiF–LiCl–LiI salt electrolyte (20:50:30 mol%, $T_m = 430\ ^\circ C$) operating at current densities as high as 1,000 mA cm$^{-2}$ (Fig. 3) not only while discharging, but also while charging. The latter is especially useful in applications such as frequency regulation. At current densities as high as 500 mA cm$^{-2}$,

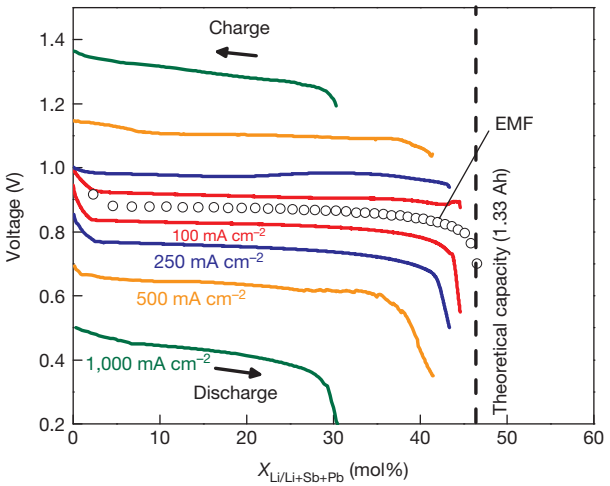


**Figure 3 | Voltage profiles during charge–discharge at different current densities (100–1,000 mA cm$^{-2}$) of a Li||Sb–Pb cell.** The theoretical capacity was 1.33 Ah with a fully discharged target composition of 45% Li in an Sb–Pb 30:70 mol% alloy (2.0 cm$^2$ of active surface area). The operating temperature was 450 °C. The results derive from measurements on more than three cells.

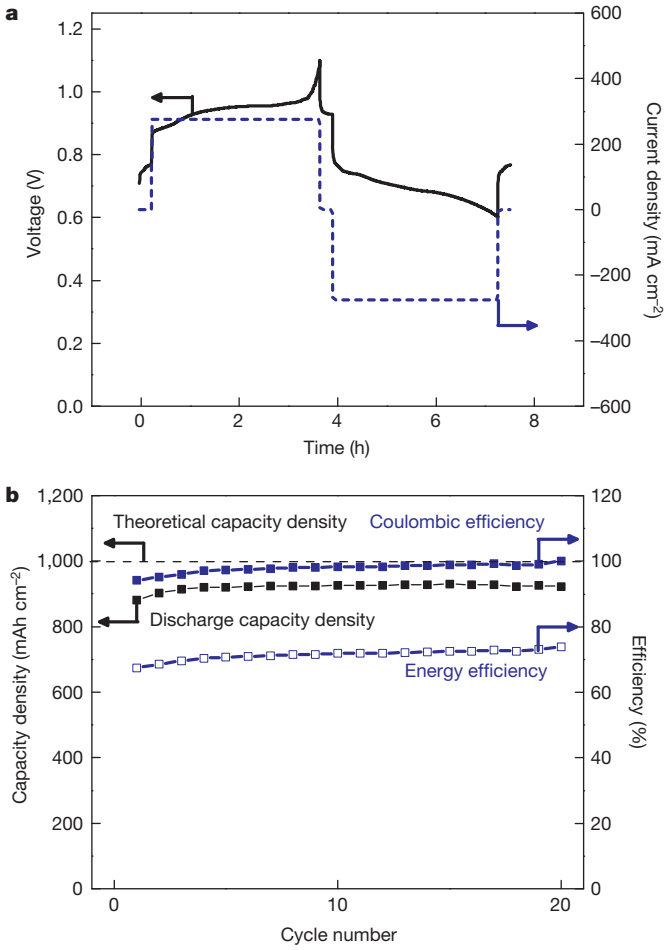


**Figure 4 | Performance of a Li||Sb–Pb cell cycled at 275 mA cm$^{-2}$.** **a**, Profiles of voltage and current density during charge–discharge (15th cycle). **b**, Coulombic efficiency, energy efficiency and discharge capacity density as functions of cycle number. The theoretical cell capacity was 62 Ah with a fully discharged target composition of 52.4% Li in an Sb–Pb 40:60 mol% alloy (62 cm$^2$ of active surface area). The operating temperature was 500 °C.

there is no significant decrease in the reversible capacity (87% of the theoretical value). Even at the highest current density (1,000 mA cm$^{-2}$), the cell performed at 54% of its theoretical capacity. Most noteworthy about this last observation is the ability of the cell to act as a high-current load without incurring permanent damage: efficiency in this instance is subordinate to long-term electrode stability. This advantageous mix of features is attributable to the rare combination of the high conductivity of the molten salt electrolyte, ultrafast charge-transfer kinetics at the electrode–electrolyte interface between the liquid metal and molten salt, and fast mass transport within the liquid metal electrodes.

To demonstrate the scalability of the system, cells with a 62 Ah theoretical capacity (62 cm$^2$) were constructed and operated with performance similar to that achieved on the smaller scale (1.9 Ah). To optimize systems costs, a LiF–LiCl–LiBr eutectic electrolyte (22:31:47 mol%, $T_m$ = 443 °C) and a positive-electrode Sb–Pb composition of 40:60 mol% were chosen. Operating at a temperature of 500 °C, the cells were cycled at 275 mA cm$^{-2}$. Figure 4 shows a typical charge–discharge voltage profile and the cell performance metrics over twenty cycles. With average values of Coulombic efficiency of 98% and a round-trip energy efficiency of 71%, negligible capacity fade was observed over the duration of the test. The nominal discharge voltage was measured to be ~0.69 V. On this basis, the electrode materials costs were estimated to be US$65 kWh$^{-1}$.

Alloying Sb with Pb has been identified as a way to achieve significant reductions in the melting point of the positive electrode as well as the cell operating temperature without an attendant decrease in cell voltage. This finding not only lowers the cost of Li||Sb–Pb batteries, increasing their attractiveness for stationary applications, but also serves as an example of how to broaden the selection of positive-electrode materials for liquid metal batteries.

**Online Content** Methods, along with any additional Extended Data display items and Source Data, are available in the online version of the paper; references unique to these sections appear only in the online paper.

**Received 12 May; accepted 21 July 2014.**
**Published online 21 September 2014.**

1. Soloveichik, G. L. Battery technologies for large-scale stationary energy storage. *Annu. Rev. Chem. Biomol. Eng.* **2,** 503–527 (2011).
2. Dunn, B., Kamath, H. & Tarascon, J.-M. Electrical energy storage for the grid: a battery of choices. *Science* **334,** 928–935 (2011).
3. Yang, Z. *et al.* Electrochemical energy storage for green grid. *Chem. Rev.* **111,** 3577–3613 (2011).
4. Barnhart, C. J. & Benson, S. M. On the importance of reducing the energetic and material demands of electrical energy storage. *Energy Environ. Sci.* **6,** 1083–1092 (2013).
5. Kim, H. *et al.* Liquid metal batteries: past, present, and future. *Chem. Rev.* **113,** 2075–2099 (2013).
6. Bradwell, D. J., Kim, H., Sirk, A. H. C. & Sadoway, D. R. Magnesium-antimony liquid metal battery for stationary energy storage. *J. Am. Chem. Soc.* **134,** 1895–1897 (2012).
7. Weppner, W. & Huggins, R. A. Thermodynamic properties of the intermetallic systems lithium-antimony and lithium-bismuth. *J. Electrochem. Soc.* **125,** 7–14 (1978).
8. Cairns, E. J. *et al. Galvanic Cells with Fused-Salt Electrolytes.* Tech. Report ANL-7316 (Argonne National Laboratory, 1967).
9. Eckert, C. A., Irwin, R. B. & Smith, J. S. Thermodynamic activity of magnesium in several highly-solvating liquid alloys. *Metall. Trans. B* **14,** 451–458 (1983).
10. Morachevskii, A. G., Bochagina, E. V. & Bykova, M. A. Thermodynamic properties of bismuth-sodium-antimony liquid alloys. *Zh. Prikl. Khim.* **73,** 1620–1624 (2011).
11. Ohtani, H., Okuda, K. & Ishida, K. Thermodynamic study of phase equilibria in the Pb-Sn-Sb System. *J. Phase Equilibria* **16,** 416–429 (1995).
12. Morachevskii, A. G. Thermodynamic analysis of alloys of the lithium-antimony system. *Zh. Prikl. Khim.* **75,** 367–369 (2002).
13. Gasior, W. & Moser, Z. Thermodynamic study of lithium-lead alloys using the EMF method. *J. Nucl. Mater.* **294,** 77–83 (2001).
14. Dworkin, A. S., Bronstein, H. R. & Bredig, M. A. Miscibility of metals with salts. VI. Lithium-lithium halide systems. *J. Phys. Chem.* **66,** 572–573 (1962).
15. Kanevskii, L. S. & Dubasova, V. S. Degradation of lithium-ion batteries and how to fight it: a review. *Russ. J. Electrochem.* **41,** 1–16 (2005); *Elektrokhimiya* **41,** 3–19 (2005).

**Acknowledgements** We acknowledge financial support from the Advanced Research Projects Agency-Energy (US Department of Energy) and Total SA.

**Author Contributions** K.W. and K.J. contributed equally to this work. K.W. and K.J. conducted equilibrium voltage measurements. K.W., K.J., T.O., D.J.B. and U.M. performed small-scale cell testing. B.C. and P.J.B. performed cell testing at engineering scale. D.R.S., D.A.B. and H.K. had the idea for the project. K.W., K.J., B.C., T.O. and D.R.S. drafted the manuscript.

**Author Information** Reprints and permissions information is available at www.nature.com/reprints. The authors declare competing financial interests: details are available in the online version of the paper. Readers are welcome to comment on the online version of the paper. Correspondence and requests for materials should be addressed to D.R.S. (dsadoway@mit.edu).

## METHODS

For all experiments, high purity (>99.9%), ultradry-grade LiF, LiCl, LiBr and LiI salts (Alfa Aesar) were used in electrolytes. Salt mixtures were dried under vacuum at 80 °C for 8 h and 250 °C for 2 h to remove residual water, and were then melted under Ar gas at 600 °C. All experiments were performed under a high-purity Ar atmosphere.

For the evaluation of equilibrium voltage by coulometric titration, all alloy target compositions were prepared using an arc-melter (MAM1, Edmund Bühler GmbH). After arc-melting, alloys were placed into a small mullite basket, pre-melted and used as working electrodes. Electrical contact was established using a tungsten wire (1 mm diameter) immersed in the Sb–Pb alloy. Ag/AgCl served as the reference electrode (3 wt% AgCl in a LiCl–NaCl–KCl eutectic mixture) and was contained within a closed-end mullite tube with the end polished to a thin microporous layer. A 40:60 mol% Li–Al alloy was used as the counter-electrode. Electrochemical measurements were performed with an Autolab PGSTAT 302N potentiostat/galvanostat.

For cell testing, galvanostatic charge and discharge were performed using an Arbin BT2000. Alloys were pre-weighed and placed in cell containers. The salt mixtures were introduced and dried *in situ* under vacuum at 80 °C for 8 h and 250 °C for 4 h before setting the operating temperature for electrochemical testing. A cell schematic of the Li||Sb–Pb liquid metal battery is shown in Extended Data Fig. 1.

All electrode cost estimations were performed using the following formula: $C = \Sigma_i P_i m_i / E$, where $C$ is the capital cost per unit of discharged electrical energy in US\$ $kWh^{-1}$, $P_i$ is the specific bulk metal cost in US\$ $kg^{-1}$, $m_i$ is the metal's mass in kg, and $E$ is the discharged energy in kWh. For Li||Sb–Pb cells, the value of discharged energy, $E$, was that measured during galvanostatic cycling at 275 mA $cm^{-2}$ (Figs 2 and 4). For Mg||Sb cells, the discharged energy, $E$, was that measured during galvanostatic cycling at 200 mA $cm^{-2}$ (ref. 6). Average bulk metal prices of Li (US\$61.7 $kg^{-1}$), Mg (UD\$2.7 $kg^{-1}$), Pb (US\$2.1 $kg^{-1}$) and Sb (US\$10.1 $kg^{-1}$) were obtained from the MetalPrices Online Database (http://www.metalprices.com literature). Detailed cost calculations for the cells are presented in Extended Data Tables 1–3. A balance of system and salt costs is not included because the technology has yet to be fully developed on the commercial scale, and so there is no accurate basis for such estimation.

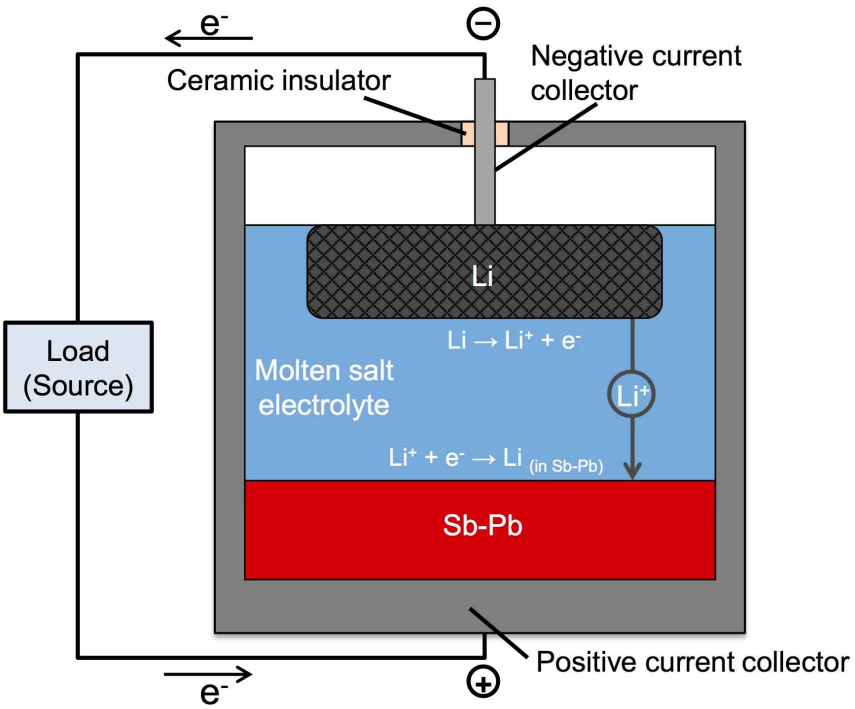


**Extended Data Figure 1 | Cell schematic of Li||Sb–Pb liquid metal battery.** The negative current collector consists of a stainless steel rod and Fe–Ni foam. The positive current collector is made of graphite (small cell; 3.16 $cm^2$ active area) or 304 stainless steel (large cell; 62 $cm^2$ active area). Current collectors are electrically isolated by means of an alumina insulator.

**Extended Data Table 1 | Cost calculation of Mg||Sb 2.5 Ah cell**

| | Mg | Sb | Total |
|---|---|---|---|
| **m /g** | 2.27 | 17.06 | 19.32 |
| **n / mol** | 0.09 | 0.14 | |
| **M / g.mol-1** | 24.31 | 121.76 | |
| **P / $/kg** | 2.70 | 10.09 | |
| **Pmolar / $/mol** | 0.07 | 1.23 | |
| **C / $/kWh** | 12.89 | 362.35 | **375.25** |
| **Energy density / Wh/kg** | | | 24.58 |
| | | | |
| **Capacity / Ah** | 2.50 | | |
| **nMg / (nMg + nSb)** | 0.40 | | |
| | | | |
| **Average discharge energy / kWh** | 4.75E-04 | | |
| **F / C.mol-1** | 96485.40 | | |

**Extended Data Table 2 | Cost calculation of Li||Sb-Pb 1.9 Ah cell**

| | Li | Pb | Sb | Total |
|---|---|---|---|---|
| **m /g** | 0.49 | 12.57 | 3.17 | 16.22 |
| **n / mol** | 0.07 | 0.06 | 0.03 | |
| **M / g.mol-1** | 6.94 | 207.20 | 121.76 | |
| **P / $/kg** | 61.70 | 2.10 | 10.09 | |
| **Pmolar / $/mol** | 0.43 | 0.44 | 1.23 | |
| **C / $/kWh** | 23.40 | 20.34 | 24.62 | **68.37** |
| **Energy density / Wh/kg** | | | | 79.96 |
| | | | | |
| **Capacity / Ah** | 1.90 | | | |
| **nLi / (nLi + nPb + nSb)** | 0.45 | | | |
| **nSb / (nSb + nPb)** | 0.30 | | | |
| **nLi / (nLi + nSb)** | 0.73 | | | |
| | | | | |
| **Average discharge energy / kWh** | 1.30E-03 | | | |
| **F / C.mol-1** | 96485.40 | | | |

**Extended Data Table 3 | Cost calculation of Li||Sb-Pb 62 Ah cell**

| | Li | Pb | Sb | Total |
|---|---|---|---|---|
| **m / g** | 16.00 | 259.80 | 101.70 | 377.50 |
| **n / mol** | 2.31 | 1.25 | 0.84 | |
| **M / g.mol-1** | 6.94 | 207.20 | 121.76 | |
| **P / $/kg** | 61.70 | 2.10 | 10.09 | |
| **Pmolar / $/mol** | 0.43 | 0.44 | 1.23 | |
| **C / $/kWh** | 25.24 | 13.95 | 26.23 | **65.41** |
| **Energy density / Wh/kg** | | | | 103.63 |
| | | | | |
| **Capacity / Ah** | 61.78 | | | |
| **nLi / (nLi + nPb + nSb)** | 0.52 | | | |
| **nSb / (nSb + nPb)** | 0.40 | | | |
| **nLi / (nLi + nSb)** | 0.73 | | | |
| | | | | |
| **Average discharge energy / kWh** | 3.91E-02 | | | |
| **F / C.mol-1** | 96485.40 | | | |